Study of Multimode Extrinsic Fabry-Perot Interferometric Fiber Optic Sensor on Biosensing

Xin Zhao

Thesis submitted to the faculty of the Virginia Polytechnic Institute and State University
in partial fulfillment of the requirements for the degree of

Master of Science
in
Electrical and Computer Engineering

Dr. Anbo Wang, Chair
Dr. Gary Pickrell
Dr. Kristie L. Cooper

August 1st, 2006
Blacksburg, Virginia

Keywords: Multimode Fiber Optic Sensors, Fabry-Perot, White-light Interferometry,
Electrostatic self-assembly (ESA), Biosensor

Study of Multimode Extrinsic Fabry-Perot Interferometric Fiber Optic Sensor on Biosensing

Xin Zhao

(ABSTRACT)

The electrostatic self-assembly (ESA) method presents an effective application in the field of biosensing due to the uniform nanoscale structure. In previous research, a single mode fiber (SMF) sensor system had been investigated for the thin-film measurement due to the high fringe visibility. However, compared with a SMF sensor system, a multimode fiber (MMF) sensor system is lower-cost and has larger sensing area (the fiber core), providing the potential for higher sensing efficiency.

In this thesis, a multimode fiber-optic sensor has been developed based on extrinsic Fabry-Perot interferometry (EFPI) for the measurement of optical thickness in self-assembled thin film layers as well as for the immunosensing test. The sensor was fabricated by connecting a multimode fiber (MMF) and a silica wafer. A Fabry-Perot cavity was formed by the reflections from the two interfaces of the wafer. The negatively charged silica wafer could be used as the substrate for the thin film immobilization scheme. The sensor is incorporated into the white-light interferometric system. By monitoring the optical cavity length increment, the self-assembled thin film thickness was measured; the immunoreaction between immunoglobulin G (IgG) and anti-IgG was investigated.

Acknowledgments

I would first like to to express my deep gratitude and sincere appreciation to my advisor, Dr. Anbo Wang, for his continuous guidance, inspiration, support, and encouragement. Throughout my study and research at Virginia Tech, he has been a wonderful professor and afforded me great opportunities in this area.

I am also deeply indebted to Dr. Gary R. Pickrell for his guidance, comments, and willingness to serve as my committee. A special thank goes to Dr. Kristie L. Cooper for her assistance in both research and technical writing throughout this project. Also thank her for being supportive all the time.

I would like to extend my acknowledgment to the group members that I have worked with during my stay at Center for Photonics Technology. Many thanks to Yizheng Zhu, who helped me out with patience, gave me encouragement and support during the project. I would also like to acknowledge Dr. Yan Zhang, who led me to fabricate the first sensor and the experiment design. I'm grateful to Xiaopei Chen, Bo Dong, Ming Han, Fabin Shen, Debbie Collins and all staff and students at CPT for their assistance and friendship.

Finally, and most importantly, I would like to say thank you to my parents, for their encouragement, support, dedication, and boundless enthusiasm for my life with their endless love.

Contents

List of Figures

List of Tables

Chapter 1

Introduction

1.1 Optical fiber sensors

Optical fiber has been involved in the sensing area for more than forty years. Optical fiber sensors have attracted a great deal of interest in a number of different fields due to their advantages such as: low loss and high accuracy; not subject to electromagnetic interference (EMI); resistance to chemical corrosion, high temperature and other harsh environments; small size, light weight, ease of installation, and capability of remote control [1]. Fiber optic sensors present advantages over conventional electrical and mechanical sensors in many ways. Basic performance could be achieved faster with higher sensitivity. Furthermore, they are more robust and flexible to be installed in harsh environments that would be impractical

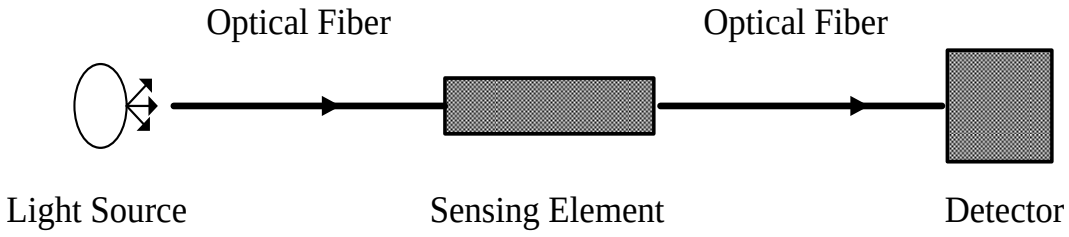

Figure 1.1: Basic scheme of an optical fiber sensor.

with conventional sensors. Figure 1.1 shows the basic arrangement of a fiber optic sensor [2].

By detecting the parameters of the light carried in the optical fiber, such as intensity, wavelength, phase, and polarization, temperature, pressure, acoustics, vibration, linear strain, humidity, chemical and biological measurements and a host of other sensor applications could be achieved.

1.1.1 Categories of optical fiber sensors

According to the sensing parameters, fiber optic sensors can be classified as four major categories: intensity-modulated sensors; wavelength-modulated sensors; phase-modulated sensors; and polarization-modulated sensors [3].

The information could be impressed in terms of intensity in an intensity-modulated sensor. For example, pressure fluctuation could be measured by a cantilevered fiber with reflective end face. Another example is microbend fiber sensors in which small bends of fiber could be sensed by detecting the change of light loss through the transducer.

In a wavelength-modulated fiber optic sensor, a light beam is modulated in wavelength by an environmental effect. Examples of these types of fiber sensors include blackbody radiation sensors, fluorescence sensors, and Bragg grating sensors. Fluorescent fiber sensors are widely used for chemical sensing and medical applications. Bragg grating sensors are extremely sensitive to mechanical strain. The grating is usually written in a fiber using an ultraviolet laser.

Polarization-modulated sensors could be used to measure electrical or magnetic field with the typical application of electrical current measurements.

Phase-modulated sensors are also called interferometric sensors, including Sagnac, Mach-Zehnder, Michelson and Fabry-Perot interferometric sensors. Among them, the most widely used is Fabry-Perot interferometric (FPI) sensor [4].

1.1.2 Fiber Fabry-Perot interferometric sensor

Fiber Fabry-Perot interferometers (FFPI) have been applied to temperature, strain, acoustic, and pressure sensing for the past two decades [5]. The Fabry-Perot interferometer consists of two parallel mirrors separated by a cavity length, through which two beams of light interfere with each other to form intensity fringe patterns. The phase of the fringe patterns is directly related to the parameters being measured.

FFPI sensors can be classified as *extrinsic* Fabry-Perot interferometric (EFPI) sensors and *intrinsic* Fabry-Perot interferometric (IFPI) sensors. When the optical fiber only plays the role of a transmission medium that guides the light to and from the sensing element, the sensor is categorized as an *extrinsic* fiber optic sensor. On the other hand, optical fiber could be used as the sensing element, which means, the Fabry-Perot cavity consisting of two reflectors is embeded in or is part of the fiber. In this case, the sensor is known as an *intrinsic* sensor.

Easy fabrication, high sensitivity, miniaturized size and low cost makes both EFPI and IFPI sensors important in sensing area. Most of the effort of optical fiber Fabry-Perot sensing has been devoted to measurands including temperature, strain, pressure, humidity, magnetic field, and flow rate.

1.1.3 Optical fiber sensors in biomedical application

Optical fiber became a key element in biomedical instruments in the 1960's. It has had great success in the applications of endoscopic imaging, laser surgery and therapy, and medical sensing. In 1970's optical fiber sensors began to develop for biomedical applications. One example is optical fiber temperature monitoring in special therapies such as hyperthermia [6], which is one of the most popular treatments that raise the temperature of the target tissue to a certain level and kill the cell. Temperature sensors, especially invasive sensors, are necessary for temperature monitoring in the tissues. Optical fiber sensors are electromag-

netic insensitive, which meets the requirement of the therapy. It also should be suitably miniaturized as an invasive sensor.

Pressure sensing is another main medical application of optical fiber sensors. A pressure sensor is usually used to measure blood pressure [7], and also, can be used in neurology and neurosurgery [8]. Humidity and air flow sensors are mainly used in breathing diagnostics [9].

Optical fiber sensors are also widely used in medical imaging such as an accessory used in Computer Tomography [10]. In cardiovascular and intensive care, it could be use to detect the oxygen saturation, blood gases and pH [7]. In the area of dermatology, it can also be used to detect the skin condition.

The medical applications of optical fiber sensors have been developed for almost half of a century. The attractive advantages such as low cost, light weight, small size, and immunity to electromagnetic interference of optical fiber sensors make them widely accepted in this field.

1.2 Introduction to biosensors

Since the first biosensors were reported in the early 1960s [11], rapid development of a wide variety of biosensors has been seen in the major areas of biological monitoring, biomedical diagnostics and environmental sensing applications.

1.2.1 Definition

A biosensor is a type of sensor often used in bioanalysis. The device for the detection of analyte consists of a sensitive biological element, often called a bioreceptor, a transducer, and a detector element [12]. Biological information is detected by the bioreceptor upon the interaction of the target analyte with the bioreceptor with a high degree of selectivity. The information is then translated by the transducer directly associated with the bioreceptor

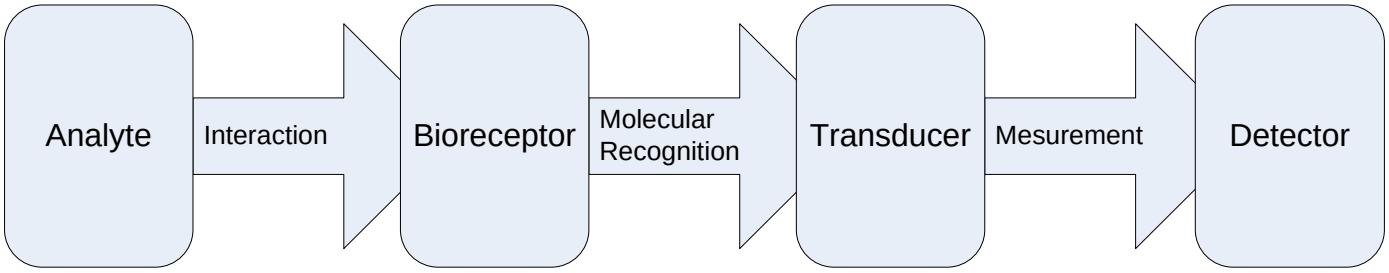

Figure 1.2: Diagram of biosensing principle.

into a certain measurable signal such as an electrical signal, or an optical signal before it is received by the detector element. Figure 1.2 schematiclly illustrates the principle of the biosensing process.

1.2.2 Classification

According to the bioreceptor type and the transducer type, biosensors could be classified by two ways [13]. The classification scheme is shown below in Figure 1.3.

A bioreceptor can be an antibody, an enzyme, a protein, or a nucleic acid or a living biological system such as cells and tissue. In a bioreceptor, the biochemical mechanism is employed as a recognition element. The bioreceptors can take different forms as different analytes are monitored. For bioreceptor classification, five different major types are used: (1) antibody/antigen-based, (2) nucleic acid/DNA-based, (3) enzyme-based, (4) cellular structure/cell-based, and (5) biomimetic-based.

Antigen-antibody (Ag-Ab) binding reaction is the key sensing mechanism by which the analyte is detected by the antibody bioreceptor due to the highly specific binding nature of an antibody and its unique antigen. The antibody/antigen-based structure is most widely

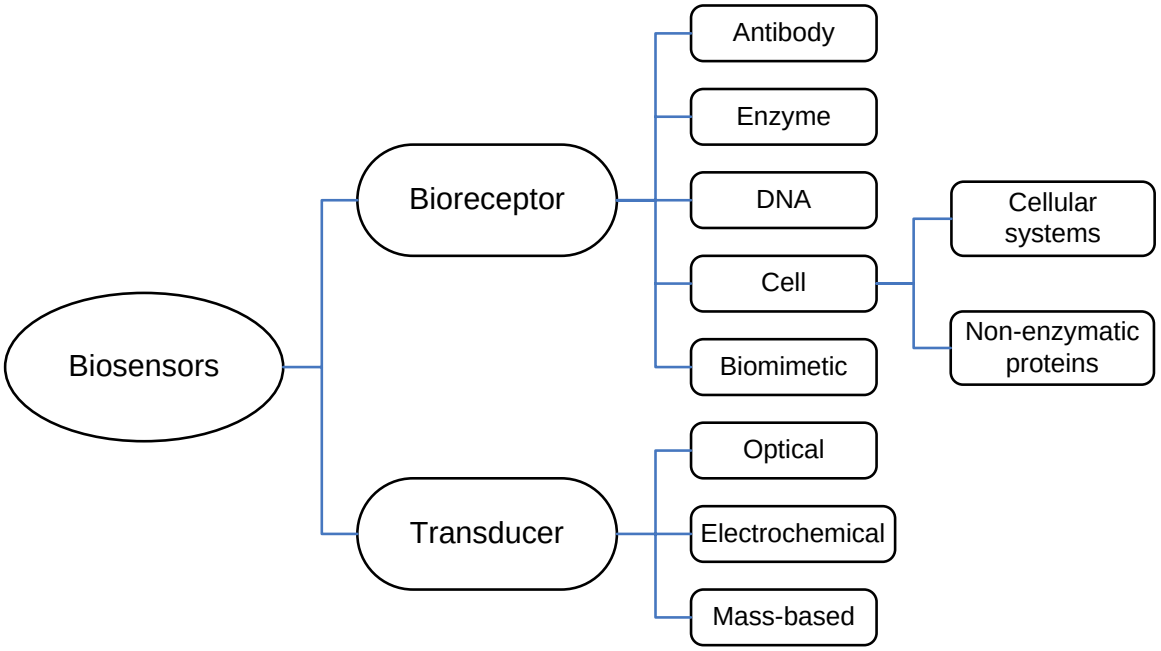

Figure 1.3: Biosensor classification schemes.(Ref. [13].)

used in bioreceotor. Besides, hybridization of DNA or RNA is also involved in recognition mechanism due to the base pairing.

Biosensors can also be categorized based on the transduction methods including: (1) optical detection methods, (2) electrochemical detection methods, and (3) mass-based detection methods.

For the optical detection methods, parameters such as amplitude, energy, polarization, decay time, and phase of target analyte could be measured with with different types of spectroscopies including absorption, fluorescence, phosphorescence, Raman, surface-enhanced Raman scattering (SERS), refraction, and dispersion spectrometry. Among them, fluorescence is the most sensitive and widely used spectroscopic techniques [13]. Electrochemical detection usually relies on the measurement of a paticular species' chemical potential, which has been extensively used in biosensors. Mass-bassed method is the newest of the three. It utilizes a kind of piezoelectric crystal with the application of an electrical signal of a specific

frequency. The crystal changes its oscillation frequency when the crystal's mass changes due to binding of chemicals such as DNA fragments or antibody. The mass change can then be measured electrically.

1.2.3 Optical fiber biosensor

When optical fiber technology is involved in the biosensing element, the biosensor could be referred to as an optical fiber biosensor. In this case, the transduction method is optical detection. As introduced in Chapter 1.1.2, optical fiber sensors could be categorized as extrinsic and intrinsic based on the function of optical fiber. Consequently, an optical fiber biosensor could be obtained either when fiber is serving only as a waveguide or when biological recognition element is directly immobilized to the fiber to form a sensing element.

1.3 Objective and outline

In previous research carried out in CPT, single mode fiber optic multicavity FPI (MFPI) sensors have been designed and developed for ESA thin film measurement and immunosensing [14]. The feasibility of using SMF-based sensors as biosensors has been verified. In spite of the high fringe visibility that could be achieved, SMF-based sensors have such inconveniences as: small detection area (the core of SMF sensor) and expensive CTS system set up. Multimode fiber sensors have larger core size consequently enlarging the detection area. Also, the white-light detection system for MMF sensors is rather low-cost.

MMF sensors have the drawback of difficult in getting high fringe visibility. However, this problem could be easily solved by using wafer-based MMF sensor, which will be specifically talked later.

In this research, a wafer-based multimode fiber (MMF) extrinsic Fabry-Perot interferometric (EFPI) senor was developed. Surface modification by the electrostatic self-assembly

(ESA) method, which provides a precursor film for supporting and protecting protein from being denatured, is applied before the binding of the receptor. Antibody is immobilized as the receptor onto the sensor head, allowing the sensor to be capable of immunosensing. When interaction between the target analyte and the bioreceptor occurs, the information is converted into optical signal by the MMF-EFPI sensor, transmitted through the fiber, detected, and then measured by the computer.

The goal of the report is to describe the fabrication and evaluation of the ESA-based multimode optical fiber sensor; provide a better understanding of the electrostatic self-assembly (ESA) thin film process on the sensor head; and present a detailed analysis on the immunobinding test using the sensor interrogated by an Ocean-Optics spectrometer-based white-light interferometry system. The MMF sensor system has the advantage of being less sensitive to bending, low cost.

The first chapter briefly reviews the research background of fiber optic sensors and biosensors. The fiber Fabry-Perot interferometric (FFPI) sensor is introduced. The application of optical fiber sensor technology in biomedical area, as well as the classification of biosensors, is reviewed.

Chapter 2 presents a discussion on principles behind the fiber-optic sensor, including a detailed description concerning Fabry-Perot interferometry theory and the process of sensor fabrication. Also presented is the improvement of the fabrication process.

Chapter 3 deals with the signal processing for the sensor and system: the experimental setup, white-light system and signal analysis.

The detailed ESA process as the surface modification is described in Chapter 4. The thickness of the thin film deposited on the surface of the MMF-EFPI sensor head is measured with high resolution.

In Chapter 5, the final procedure of the biosensor fabrication, which is referred to as the bioreceptor immobilization, is presented. The specific binding, as well as the nonspecific

binding, is investigated. The feasibility of using the multimode fiber FP sensor as a biosensor is verified. The binding tests are examined when binding block is both applied or not. The requirement of binding block is also proved.

Finally the thesis is summarized and recommendations for future research are suggested in Chapter 6.

Chapter 2

Multimode extrinsic Fabry-Perot interferometry sensor

2.1 Introduction to MMF-EFPI sensor

Interferometer technologies, including Mach-Zehnder, Sagnac, Michelson and Fabry-Perot (FP) interferometers, have become widely accepted in the area of fiber optic sensors. Fiber optic sensors based on the Fabry-Perot interferometer have received more attention because they provide many advantages over other interferometric sensing schemes, such as small size, high sensitivity, point sensing, polarization independence, and multiplexing capacity [15].

Fabry-Perot Interferometry

As mentioned in Chapter 1.1.2, FFPI sensors include *extrinsic* Fabry-Perot interferometric (EFPI) sensors and *intrinsic* Fabry-Perot interferometric (IFPI) sensors. However, EFPI sensors are more popular. Many types of EFPI fiber optic sensors have been designed and implemented in the applications of sensing a variety of measurands.

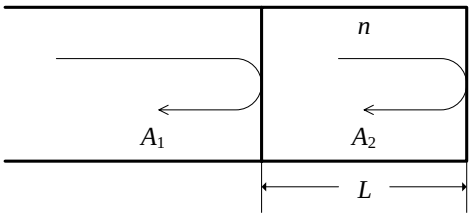

Figure 2.1: Basic structure of a Fabry-Perot Interferometer.

The Fabry-Perot interferometer (FPI) is a simple device that relies on the interference of multiple beams [16]. The interferometer consists of two parallel semi-transparent reflective surfaces that are well aligned to form an optical Fabry-Perot cavity with cavity length L and refractive index n. When a monochromatic input light enters the Fabry-Perot cavity, two reflections at the two surfaces with amplitudes of A_1 and A_2 are generated respectively. Thus, the two reflections interfere with each other to produce an interference pattern consisting peaks and valleys as some light constructively interferes and some destructively. The total reflected light intensity can be written as follows for low-finesse:

$$\begin{aligned} I &= A_1^2 + A_2^2 + 2A_1A_2\cos(\Delta\phi) \\ &= A_1^2 + A_2^2 + 2A_1A_2\cos(\frac{4\pi nL}{\lambda}), \end{aligned} \tag{2.1}$$

$\Delta\phi$ is the relative phase shift between the two light signals. λ denotes the wavelength of the interrogation light source. The basic principle of Fabry-Perot interferometric sensors is quite clear: Changes in the FP cavity length produce a cosine modulation of the output intensity signal. The change of the physical parameter under measurement is converted into a change in the cavity length L and subsequently modifies I. Therefore, those physical parameters changes could be obtained by examining I.

MMF-EFPI sensor

Multimode fiber (MMF) can be implemented in an extrinsic-FPI (EFPI) fiber optic sensor to form a MMF-EFPI sensor. MMF-based EFPI sensors have drawn less interest in research and industrial production than single mode fiber (SMF)-based sensors due to the difficulty of obtaining high fringe visibility in MMF-EFPI sensor fabrication. However, the great potential for cost efficiency of the MMF-EFPI system should not be ignored. In addition, when using as a biosensor, MMF-EFPI sensors have the advantage of a larger sensing area (the core size) compared with SMF-EFPI sensors.

Fringe visibility is also called fringe contrast. The fringe visibility of an EFPI sensor is defined by

$$V_b = (I_{max} - I_{min})/(I_{max} + I_{min}), \tag{2.2}$$

where I_{max} and I_{min} are the maximum and minimum spectral intensities in the spectral fringes from the EFPI sensor. Fringe visibility is one of the most important parameters that characterize the performance of an EFPI sensor since the ultimate signal-to-noise ration (SNR) of the system is largely determined by it. Parameters that influence the fringe visibility include: the sensor head structure, the fiber parameters, and the mode power distribution in the MMF of the sensors.

MMF contains a number of different propagation modes due to their large diameter and large numerical aperture (NA), therefore, good interference is difficult to generate in MMF-EFPIs [17]. The fringes are very sensitive to the smoothness, the flatness, the distance and especially the parallelism of the two surfaces [18]. Even an angle on the order of 10^{-2} degree could significantly reduce the fringe visibility [19]. However, fringe visibility largely determines the ultimate signal-to-noise ratio (SNR) of the system, and is one of the most important parameters that characterize the performance of an EFPI sensor [20]. The difficulty of obtaining high fringe visibility is one drawback for the MMF-EFPI sensor and need to be solved.

This problem can be solved with a wafer-based MMF sensor in which high quality silica wafers are commercially available. Since high surface quality and excellent parallelism can be readily achieved in the current wafer lapping/polishing industry, fringes can be easily generated even for highly multimoded fiber and large cavity length (thick wafer).

The silica wafers used in this research have excellent surface quality and parallelism. Good interference can be generated in the FPI formed by the two surfaces of the wafer. High fringe visibility therefore can be easily achieved. In addition, great convenience to the signal processing can also be obtained.

2.2 Sensor fabrication

A MMF-EFPI sensor has been developed. The sensor was fabricated by connecting a multimode fiber (MMF) to a silica wafer with a section of glass tube. A Fabry-Perot cavity was formed by the reflections from the two wafer interfaces. The fabrication process is described as below.

1. A $50\mu m$-thick fused silica wafer (Valley Design Corp.) of size $1\ mm \times 1\ mm$ was bonded onto the end of a well cleaved glass tube with sol-gel. The surfaces of both the wafer and the end of the tube should be flat and smooth.

2. Sol-gel was applied to seal the joint of the wafer and the tube.

3. By cleaving and inserting a multimode fiber into the tube, a Fabry-Perot cavity was formed with the fiber-to-wafer interface and the wafer-to-air interface.

4. Epoxy adhesive was used to connect the fiber and the tube.

The silica wafer on the sensor head not only functioned as a part of the Fabry-Perot cavity, but also played the role of the silica substrate to form electrostatic self-assembled

(ESA) thin films (Chapter 4), in turn enabling the MMF sensor to be a biosensor. Therefore, both surfaces of the wafer should be clean.

Improvement

Since later the sensor would be immersed in solutions for all the biosensing experiments, step 2 is required to prevent water getting into the sensor to damage it. As you can see, sol-gel was first used for this purpose. However, it was easily destroyed by the corrosive acid when being exposed in "piranha solution" (Chapter 4). This problem was solved by using glass powder instead of sol-gel to seal the joint, resulting in a robust and durable sensor with small size.

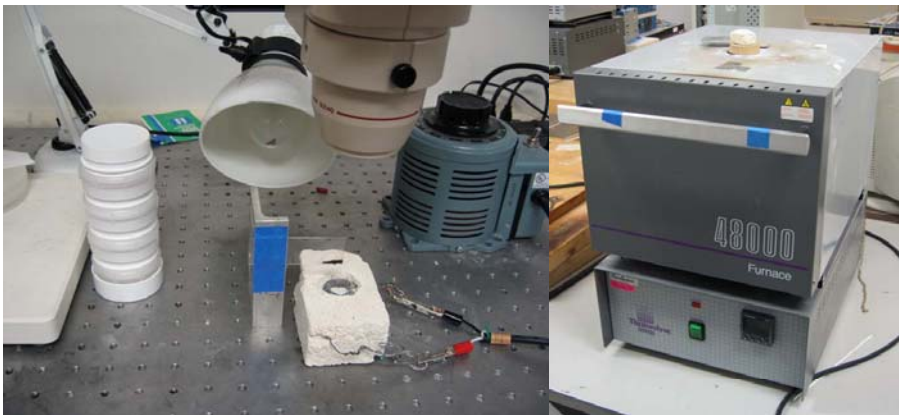

Figure 2.2: The setup for sensor fabrication (From left: glass powder, table lamp, microscope, resistive wires, transformer, and furnace).

The whole experiment setup for sensor fabrication is shown in Figure 2.2. Glass power, borosilicate glass with a softening point around 800^oC, was used for the sealing process in stead of sol-gel (Step 2). Use resistive wires and a transformer to make a small oven, then place the solgel-bonded wafer/tube over the oven. Through a microscope the glass power was carefully applied around the joint, and turn on the oven to melt the glass. At the same time, monitor the process through microscope until the glass was melted and fully cover to

seal the joint. Then reduce the transformer voltage to slowly cool down the sensor to prevent the glass from breaking. The Thermolyne 48000 furnace was for solgel bonding and epoxy bonding of the sensor parts in Step 1 and Step 4. The whole fabrication process is illustrated in Figure 2.3.

After the improvement, the sensor was capable of applying in piranha solution since glass powder is resistant in corrosive acid. The sensor was then reusable. The repeatability of the experiment is verified later.

The sensor was interrogated by the Ocean-Optics spectrometer-based white-light system, which will be discussed together with the signal processing in the next chapter. ESA process will be applied on the sensor head subsequently (Figure 2.5): after pirahna bath, the surface of the silica wafer of the sensor head will be negatively charged and suitable for ESA process as a substrate.

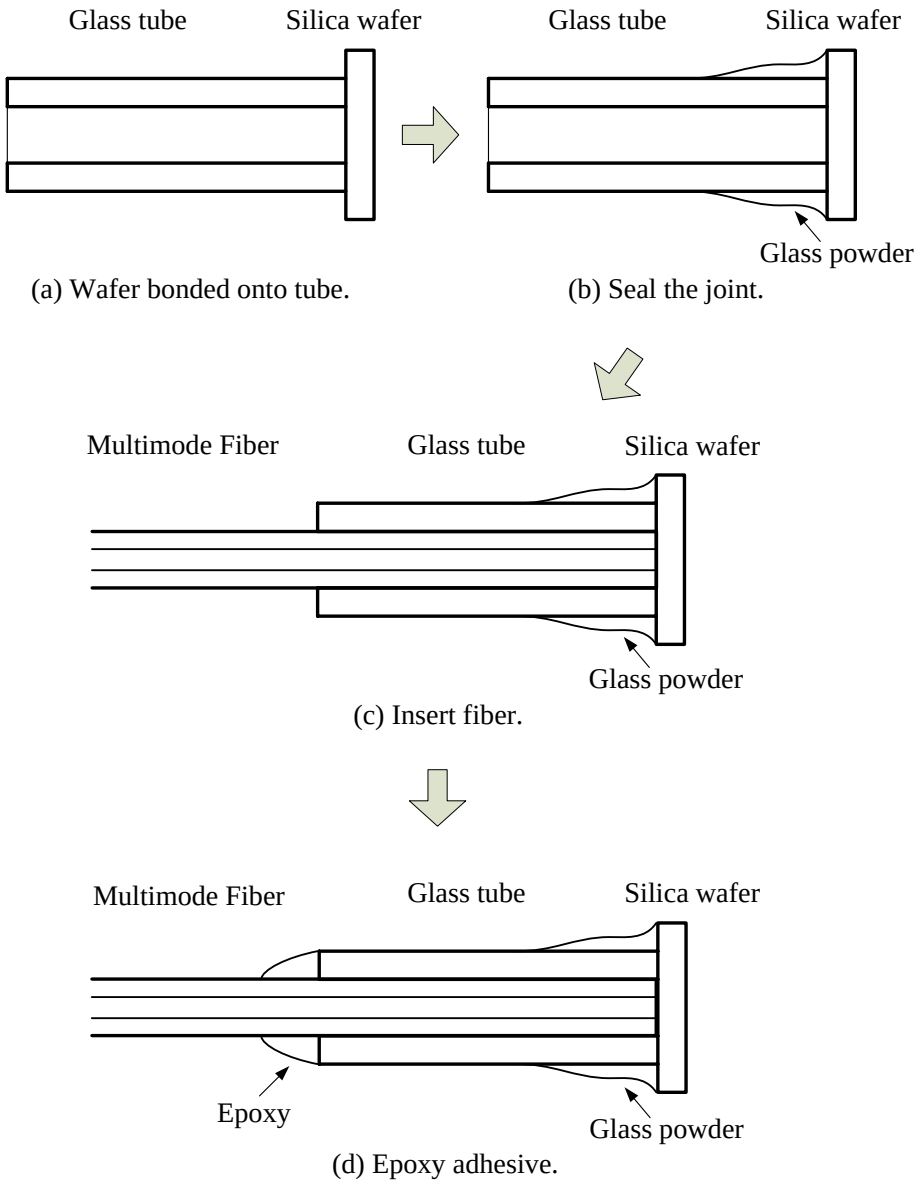

Figure 2.3: Procedures in MMF-EFPI sensor fabrication.

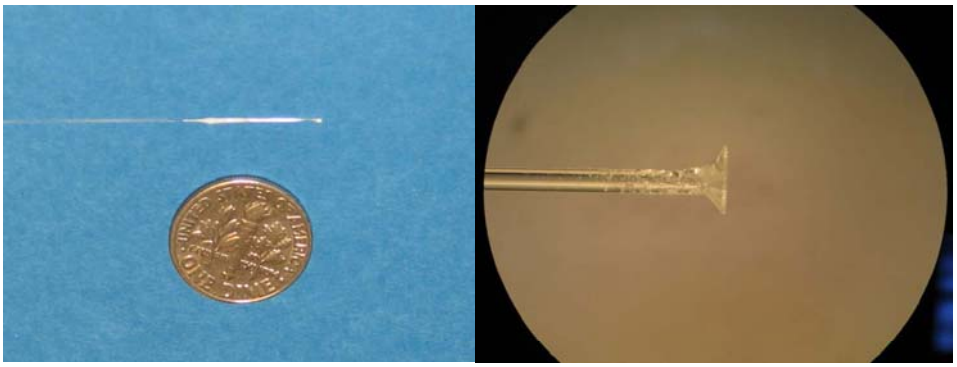

(a) The sensor compared with a dime.

(b) Sensor head under a microscope.

Figure 2.4: Pictures of the MMF-EFPI sensor.

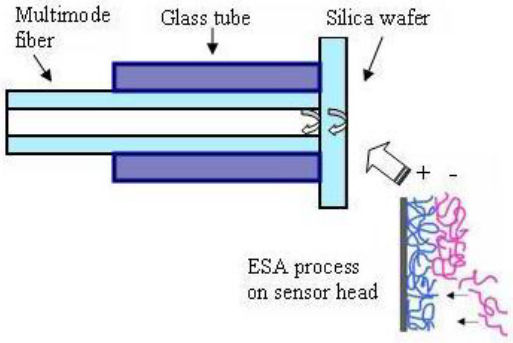

Figure 2.5: The structure of the MMF-EFPI sensor.

Chapter 3

Signal processing

Interferometric sensors constitute one of the major categories in the field of fiber-optic sensing with high resolution. These sensors are essentially interferometers which generate multiple beams of light to interference with each other. In this chapter, the principle of white-light interferometry is introduced, as well as the interferometric systems. Also discussed are the basic white-light signal processing and the algorithm.

3.1 Experimental setup and white light system

In a typical white-light interferometric system, a 850 nm LED (60 nm bandwidth) was used as the broadband light source. The interference spectrum was measured by a compact USB2000 fiber spectrometer (Ocean Optics) [21]. The light emitted from the broadband source travels through a 3-dB directional coupler to the sensing interferometer, which senses the environmental physical changes, encodes the information into the incoming light, and reflects it back to the processing unit for detection. Another end of the coupler is index-matched to prevent any reflection.

In the optical processing unit, a spectrometer was used to retrieve the spectrum of

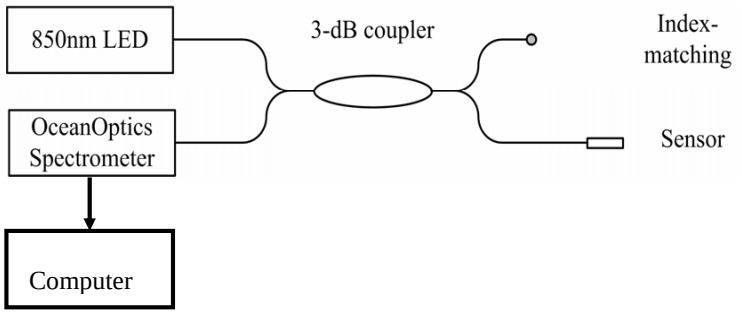

Figure 3.1: The scheme of white-light interferometric systems.

Figure 3.2: The picture of the Ocean-Optics spectrometer-based white-light interferometry system.

the reflected broadband light. Direct spectral analysis can then resolve the environmental physical change. This method is getting more and more attentions and shown to be very effective, accurate, and robust for practical industrial applications. The measured spectrum is transferred to a computer for data processing.

3.2 Signal analysis

3.2.1 Signal processing methods

As mentioned in Eq. 2.1,

$$I = A_1^2 + A_2^2 + 2A_1A_2\cos(\frac{4\pi nL}{\lambda}),$$

Determining cavity length L accurately is essential to the system performance. In this section, two methods are discussed, namely, fringe-spacing demodulation and fringe-tracing demodulation.

Fringe spacing demodulation

The cavity length L can be determined by the periodic FPI spectrum. The period can be calculated by the distance between adjacent peaks and/or valleys. λ_1 and λ_2, denoting the positions of adjacent peak 1 and peak 2, should satisfy the following in-phase condition [21]:

$$\frac{4\pi nL}{\lambda_1} = 2\pi N, \frac{4\pi nL}{\lambda_2} = 2\pi(N-1), \tag{3.1}$$

where N is the fringe order for peak 1. Subtracting the above two, we get

$$\frac{2nL}{\lambda_1} - \frac{2nL}{\lambda_2} = 1,$$

$$L = \frac{\lambda_1\lambda_2}{2n(\lambda_2 - \lambda_1)}, \tag{3.2}$$

By taking differential of Eq. 3.2,

$$\begin{aligned} \Delta L &= \frac{\lambda_2^2\Delta\lambda_1}{2n(\lambda_2-\lambda_1)^2} - \frac{\lambda_1^2\Delta\lambda_2}{2n(\lambda_2-\lambda_1)^2} \\ &\approx \frac{\lambda_1\lambda_2}{2n(\lambda_2-\lambda_1)^2}(\Delta\lambda_1 - \Delta\lambda_2) \\ &= \frac{L(\Delta\lambda_1 - \Delta\lambda_2)}{\lambda_2 - \lambda_1} \end{aligned} \tag{3.3}$$

so

$$\frac{\Delta L}{L} = \frac{\Delta\lambda_1 - \Delta\lambda_2}{\lambda_2 - \lambda_1} \tag{3.4}$$

where the approximation is made because λ_1 and λ_2 are usually close and approximately equal. It is also reasonable to assume that $\Delta\lambda_1$ and $\Delta\lambda_2$ are independent and the same, denoted as $\Delta\lambda$. Then we get,

$$\frac{\Delta L}{L} = \frac{\sqrt{2}\Delta\lambda}{\lambda_2 - \lambda_1} \tag{3.5}$$

Fringe tracing demodulation

Rather than calculating the relative phase difference, L could be demodulated by the absolute phase information [21]. From Eq 3.1, we have:

$$L = \frac{N}{2n}\lambda_1, \tag{3.6}$$

which does not need a second peak. Only the position of one peak or one valley and its fringe order is required. N can be pre-determined from the spectrum and monitored throughout experiment, which is referred to as "fringe tracing"

The relative error $\Delta L/L$ is inversely proportional to the the wavelength:

$$\frac{\Delta L}{L} = \frac{\Delta\lambda}{\lambda_1} \tag{3.7}$$

Compared with Eq. 3.5, the gain of resolution is:

$$\eta = \frac{(\Delta L/L)_{rel}}{(\Delta L/L)_{abs}} = \frac{\sqrt{2}\lambda_1}{(\lambda_1 - \lambda_2)} \tag{3.8}$$

There is a gain in resolution because absolute wavelength is usually much larger than the peak distance. That's why fringe-tracking is more accurate. It's also simpler than the fringe spacing method because only one peak needs to be tracked. In this research, the fringe tracing technology is used due to its excellent accuracy and resolution and simplicity. But the expense is that we need to predetermine N. Usually we use a combination of these two methods, first a fringe-spacing for a rough estimate of cavity length and N, and then use fringe-tracking for more accurate monitoring.

3.2.2 Signal analysis

The spectrum of the sensor is as Figure 3.3. As we can see, high fringe visibility is obtained. The spectrum has a high frequency component corresponding to the sensor signal, as well as a DC background: the low frequency component.

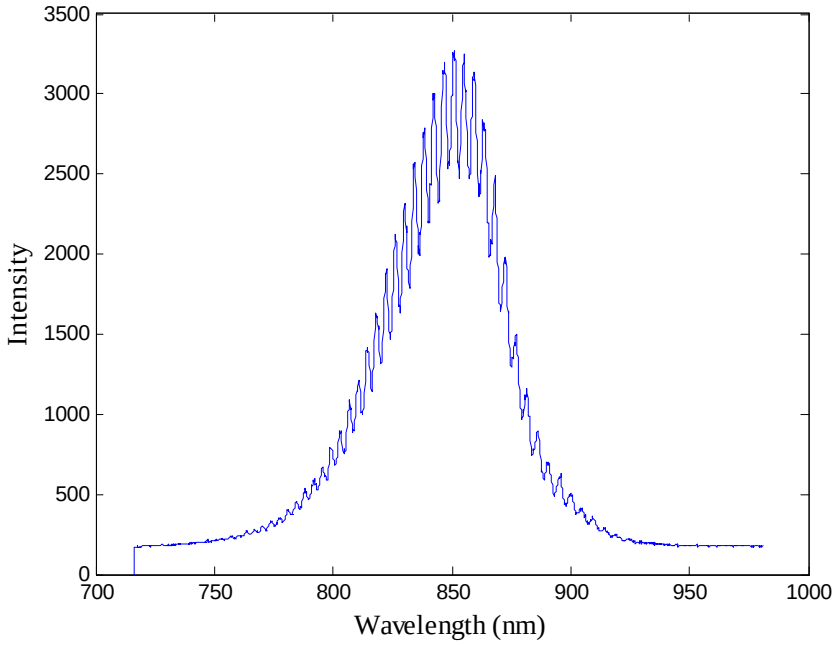

Figure 3.3: The spectrum of the MMF-EFPI sensor interrogated by the white-light interferometric systems.

Figure 3.4 shows the signal after the fast Fourier transform (FFT): the two components are clearly separated. In the Fourier transform of the spectrum, all but the interference signal (cosine term) will locate around the zero frequency. The cosine term, however, is a high frequency component and separates from the others in the fast Fourier transform.

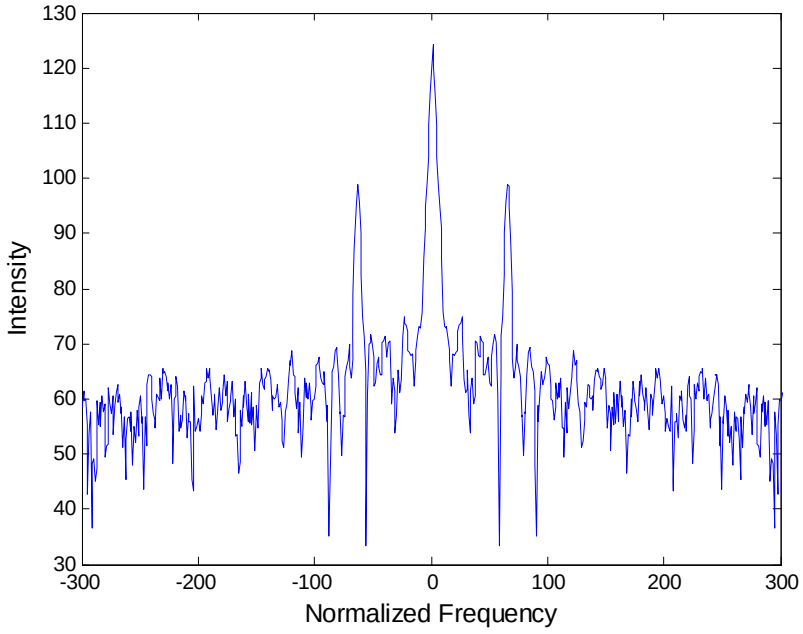

Figure 3.4: The FFT of the sensor's spectrum.

So in the signal processing, a band pass filter was used to remove the background and just extract the high frequency sensor signal. The signal is shown in Figure 3.5. And this signal still has the light source profile which needs to be removed.

Here we use Hilbert transform to extract this envelope and use it to normalize the signal. The final result is a pure cosine waveform (Figure 3.6). In the expression of the interference signal (Eq. 2.1), $A_1^2 + A_2^2$ is the DC component, $A_1 A_2$ is the envelope. Both of them are removed to get the cosine term which is only dependent on the optical cavity length nL.

Then the optical thickness (OT), the product of refractive index and thickness nL, can be monitored by spectrum-tracking technology, as introduced in Section 3.2.1. First a fringe-spacing is used for a rough estimate of cavity length and N, and then fringe-tracking is applied for more accurate monitoring. There are also other ways to analyze fringes. But they all have parts corresponding to these two methods. Basically, all these signal processing algorithms are equivalent.

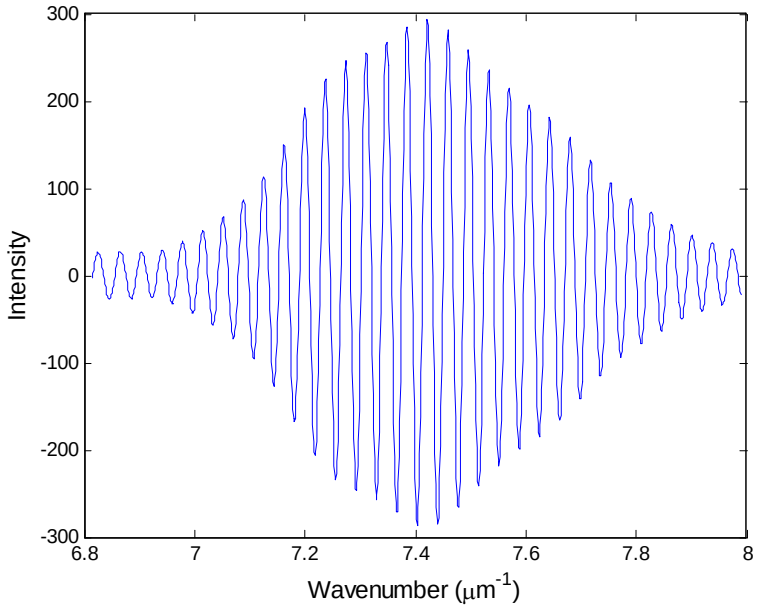

Figure 3.5: The signal after filtering.

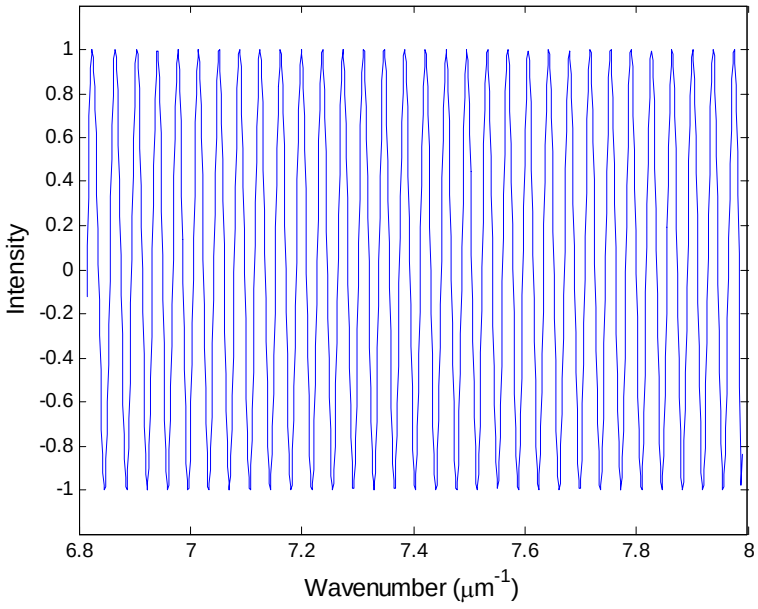

Figure 3.6: The normalize spectrum after Hilbert transform.

With this method, the thickness of ESA thin film could be measured (Chapter 4). The adsorbed thin film can be estimated as an extension of the FP cavity when the refractive index of the film is similar to the wafer. As FP cavity length increases with ESA films deposit onto sensor head layer by layer, the change of optical thickness can be monitored by the white-light system. High sensitivity can be achieved due to the intrinsic nature of Fabry-Perot interferometry.

Chapter 4

Electrostatic self-assembly process on sensor end

4.1 Introduction

The past decades have seen a great deal of progress in organic thin film fabrication technology in the application of different fields, including surface coating, MEMS, optoelectronics, nonlinear optics and sensors [22]. In the past research work, multilayer nanostructured thin films could be formed by a number of fabrication methods, among which the most commonly used processes are Langmuir-Blodgett (LB) films and self-assembled monolayer (SAM). A Langmuir film is formed on a water surface by mechanically forcing the molecules together. The resulting film can controled to be either hydrophobic or hydrophilic depending on the last deposition. SAMs are generally formed by dipping the substrate into a solution containing the molecule to be assembled. The adsorption of the layers is based on covalent reaction. These two methods have been well investigated and utilized for more than 50 years [23]. However, they have some disadvantages: LB films are limited in molecular choosing and not robust enough for many applications. As for SAMs, the fabrication process is usually time-consuming since high-yield chemical reactions are required.

The electrostatic self-assembly (ESA) method, which is based on the fabrication of molecular multilayers by the electrostatic attraction between oppositely charged polyelectrolytes, has been studied extensively in the past ten years. Compared with the LB films method and SAM method, the ESA method possesses a number of advantages as follows [24]:

- Easy to fabricate with water-based process at room temperature and pressure.
- Flexible in substrate choosing and molecular choosing.
- The detailed structure and thickness of films can be controlled.
- High quality films with excellent uniformity can be obtained.
- Excellent long-term environmental robustness and stability can be achieved.
- Broad range of applications can be found in a number of different fields.
- Low-cost manufacturing.
- Automated dipping systems could be involved.

A molecular layer-by-layer thin film structure could be easily obtained by alternately dipping the substrate into oppositely charged polymer solutions at room temperature [25]. ESA is suitable for a variety of molecules including nonlinear optical chromophores, conducting polymers, biological macromolecules, magnetic materials, dielectrics, and metallic or metallic oxide nanoparticles [24] [26]. Film thickness increases linearly at a molecular level with the number of film layers. The film structure and thickness can be affected by environmental factors such as temperature and humidity and deposition conditions. Therefore, the film structure and thickness can be controlled by parameters such as polymer concentration, pH value, substrate condition, and salt concentration in the polymer solution [27] [28].

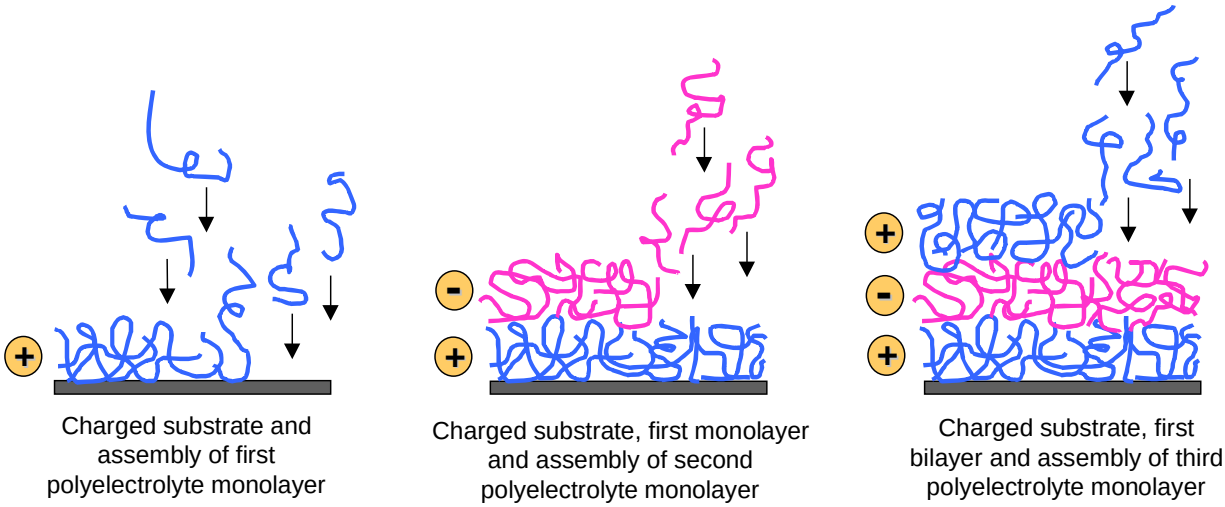

Figure 4.1: Adsorption steps of ESA method.(Courtesy of Ref. [24].)

4.1.1 Process and characterization techniques

Figure 4.1 shows the basic process of ESA. First of all, the surface of a negatively charged substrate, for example, silica wafer, should be cleaned thoroughly. Then the substrate is dipped into a polycation solution to self-assemble a uniform positively charged molecular monolayer over the negatively charged surface. After rinsing away the loose particles, a polyanionic monolayer can be adsorbed in much the same way. By alternately depositing polycationic and polyanionic monolayers onto a charged substrate, bilayer pairs can be formed electrostatically at the nanometer level.

Several analysis tools can be applied to characterize the ESA thin films, allowing the uniformity, film thickness, layer-by-layer linearity, surface morphology, thermal properties and optical characteristics to be determined [24]:

- Ellipsometry
- UV/vis spectroscopy

- Atomic force microscopy (AFM)
- Contact angle
- Fluorescence spectroscopy

Due to the easily-achieved uniform nanoscale structure, the ESA method provides effective applications in the fields of linear and nonlinear optical thin films, optics, electronics, and biosensing.

4.1.2 ESA in surface modification

ESA is an effective tool in surface modification. In biosensor development, activity of biological recognition element (the bioreceptor) is highly demanded since it is the key sensing element associated with the performance of the sensor. However, in many cases when been directly bound to solid surfaces, the biomolecules have denatured in the process of adsorption [29]. Their hydrogen-bonded configuration is broken by the forces that flatten the molecules against the surface without a proper precursor film been applied [30]. In this way the biomolecules will lose their biospecific activities. Therefore, before the protein immobilization, surface modification by ESA method is required to preserve the biological activity of the bioreceptor although protein could be adsorbed onto the silica surface directly.

The effect of the surface modification process is not only to form a "soft" surface for the immobilization of antibodies, but also had been demonstrated to increase the capacity of the sensing thin film to bind subsequent antibodies through the fabrication of a multilayer antibody film [31]. In this research, only the first purpose will be discussed.

4.2 Polyelectrolyte self-assembly on sensor head

4.2.1 Materials and methods

Materials and solution preparation

Table 4.1: The materials used in the experiment.

Material		Detail	Company
Film component	PAH	Polyallylamine hydrochloride	Aldrich
	PSS	Polysodium 4-styrenesulfonate	Aldrich
Substrate	silica wafer	50 μm in thickness	Valley Design Corp.

Details of film components and substrate are listed in Table 4.1. PAH was used as the cationic polymer, while PSS was used as the anionic polymer. The ultrapure water used for all experiments and cleaning procedures was obtained from a Barnstead Nanopure Diamond system, with a resistivity greater than 17 $M\Omega \cdot cm$. The salt concentration was adjusted by NaCl. A Corning 455 Ion Analyzer with ATC probe was used to adjust pH values with HCl and NaOH. The substrate is the 50-micron silica wafer on the sensor head, which is described in Chapter 2.2. All experiments were carried out at room temperature. The list below presents the procedure of solution preparation.

1. Dissolve the polymers in ultrapure water, add in NaCl. Details are shown in Table 4.2.
2. Stir the solutions overnight.
3. Adjust pH value.
4. Prepare piranha solution, a 30:70 mixture of 30% hydrogen peroxide (H_2O_2) and concentrated sulfuric acid (H_2SO_4), for substrate modification [24].

Table 4.2: The preparation of polymer solutions.

Polymer	**Volume**	**Concentration**	**Salt Concentration**	**pH**
PAH	20 ml	4 mg/ml	0.15 M	7.5
PSS	20 ml	4 mg/ml	0.15 M	7.5

Previous works have shown that polymer species and salt concentration are the dominant factors that affect S/N ratio in thickness [14]. PAH was chosen as the cationic polymer specie and 0.15M (NaCl) in salt concentration was selected for the following experiments since those levels result in higher S/N ratios for thin film thickness in statistical analysis. pH values were adjusted to 7.5 according to the requirement of future immuno-experiment.

ESA processing procedure

"Piranha bath" was applied for the substrate modification. The sensor head was immersed into the piranha solution at room temperature for 1 hour, followed by thorough rinsing with ultrapure water with an ultrasonic agitator, and dried in nitrogen.

The cationic layer PAH was first self-assembled onto the negatively charged silica wafer, the substrate, on the sensor head. The sensor was immersed in the PAH solution for 6 min and then was rinsed by the ultrapure water with an ultrasonic agitator for 2 min. The sensor was dried and measured immediately. Same procedure was followed for the PSS anionic layer to complete a bilayer pair. A total of 10 bilayers were obtained by alternately dipping the sensor in the polycationic solution and the polyanionic solution. The experimental setup is as simple as in Figure 4.2. The sensor is connected with a white-light system and interrogated by a computer.

Figure 4.2: Experimental setup for ESA process.

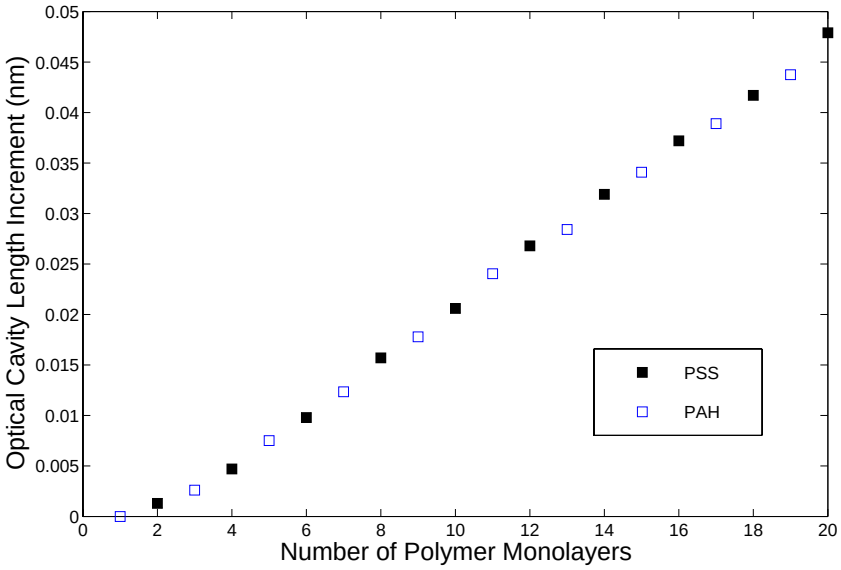

Figure 4.3: Optical thickness increases with the experiment steps.

4.2.2 Results and analysis

$[PAH/PSS]_n$ film was deposited onto the silica wafer of the sensor head. As described in Chapter 3.1, the film thickness for each layer was measured by the MMF-EFPI sensor, which was interrogated by the Ocean-Optics spectrometer-based white-light interferometry system. Figure 4.3 shows the steps of the experiment and the thickness change of the self-assembled polymer layers. 10 bilayers were obtained.

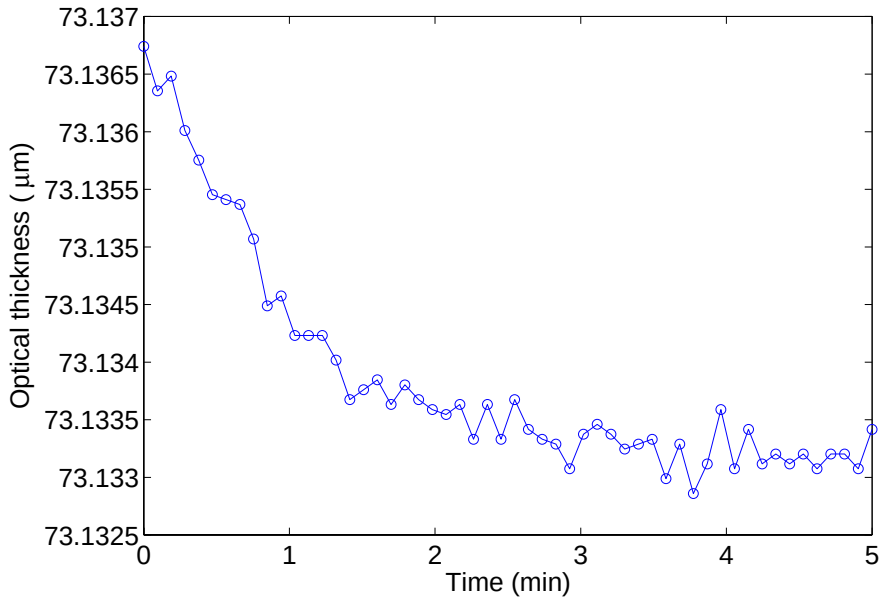

Figure 4.4: Optical thickness change in the first five minutes after dry.

Drying time After taking the sensor out of the ultrasonic rinsing, a certain amount of time is required to let the sensor dry completely. Although the sensor can get dried quickly in the air, the data is not steady for a few minutes. It may drop a little due to the evaporation of the water which is not completely dried. Figure 4.4 shows the thickness change during the first five minutes a 5-PAH/PSS-bilayer-coated sensor was taken out of ultrapure water. The figure illustrated that data tend to be steady after 2 minutes. Therefore, 2 minutes' drying time was applied in the experiment procedure to get a more reliable data.

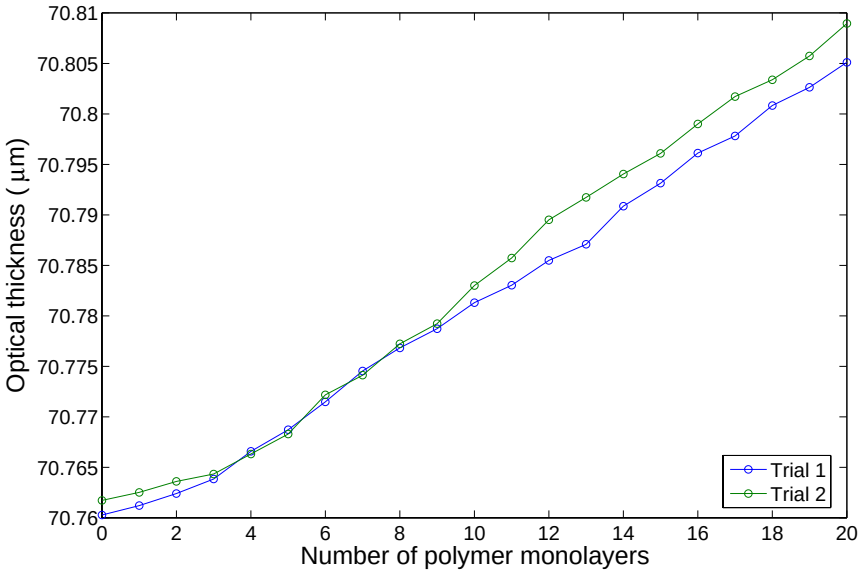

Figure 4.5: Optical thickness changes with the number of PAH/PSS layers.

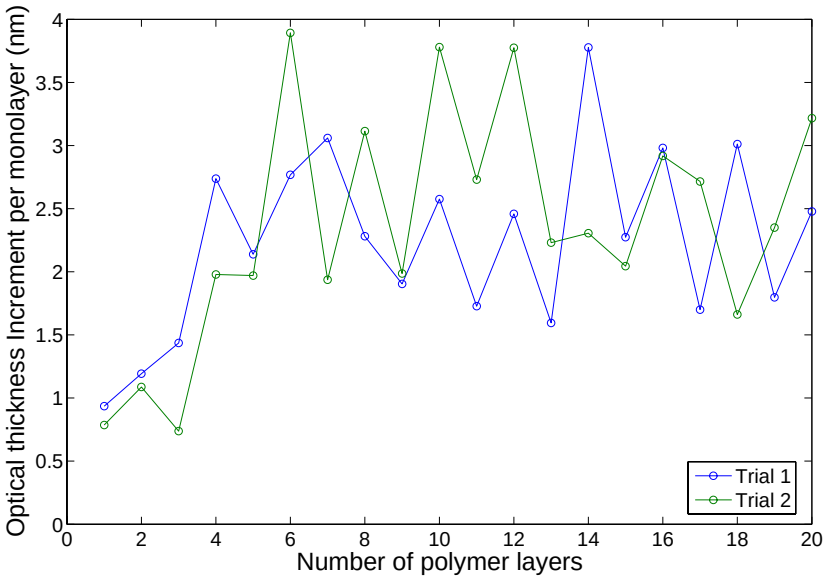

Figure 4.6: Dependence of monolayer thickness on number of polymer monolayers (alterating PAH/PSS).

Film thickness The reflection from the silica-film interface is negligible in the simplified analysis due to the similar refractive index of the polymer film and the silica wafer [14]. Consequently the silica-film cavity length could be used to estimate the optical thickness of the thin film. Optical thickness is the product of thickness in nm and refractive index n (n=1.54, measured by ellipsometry).

Figure 4.5 shows the changes in optical thickness of polymer self-assembled $[PAH/PSS]_{10}$ measured by the MMF-EFPI sensor. The average thickness per bilayer is 4.6±0.8 nm, in which the thickness of PAH and PSS layer are not the same. The average thickness of a PAH layer is 1.9±0.6 nm, which is thinner than that of a PSS layer (2.7±0.8 nm). This result is similar to that of the previous research [14].

Repeatability Also we can see from Figure 4.5, the results of the two trails is quite similar, indicating that the experiment is repeatable. For both of the two trails, the first layers are thinner relative to subsequent regular-thickness layers. After the first two bilayers, the film thickness tends to increase linearly with the bilayer number. There is also good repeatability on average film thickness.

4.3 Conclusion

In this chapter, the ESA method and procedure were introduced. Polymer thin films were fabricated successfully onto the end of a MMF-EFPI sensor using the ESA process with good repeatability. The thickness of the thin films was measured by the sensor and the white-light system with high sensitivity. Average film thickness of each layer on the sensor head was obtained. Combined with the ESA technology, MMF sensor was demonstrated to be an effect tool in thin film fabrication and examination.

The high sensitivity of the MMF-EFPI sensor provides the possibility for sensing immunoreactions at the interfaces. The self-assembled thin films could be employed as a pre-

cursor film for biosensing. Due to the requirement of surface modification in fiber optic biosensing, ESA provides a safe substrate for protein immobilization without damaging the biological activity. The effect of ESA thin films on immunosensing will be further discussed in the next chapter.

Chapter 5

Antibody immobilization and antigen binding

5.1 Introduction

An antigen is a substance that stimulates an immune response, especially the production of antibody. An antibody is a protein used by the immune system to identify and neutralize foreign objects that can recognize a specific antigen unique to its target. Antigen/antibody-based biosensor has drawn a great deal of research interest in the biosensing area due to the high selectivity of antigen/antibody (Ag-Ab) binding reaction. The immobilization of antibody could make the fiber optic sensor capable of immunosensing because of the biological recognition element.

Antibody and IgG

Each antibody recognizes a specific antigen due to its unique structure. Immunoglobulins are glycoproteins in the immunoglobulin superfamily that function as antibodies. Immunoglobulin G (IgG) is a large Y-shaped protein in an organism used by the immune system to

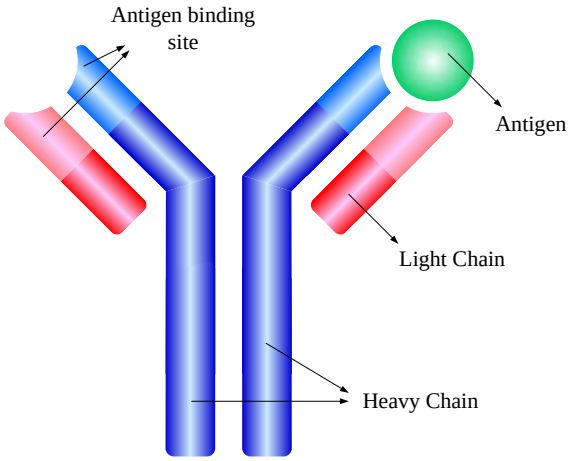

Figure 5.1: The structure of an IgG.

identify and neutralize foreign objects like bacteria and viruses [32]. An IgG consists of two heavy chains γ and two light chains. Each molecule has two antigen binding sites. IgG molecules have three protein regions: two Fab (fragment antigen binding) fragments and a Fc (fragment crystallizable) fragment. Two Fab fragments are receptor sites that recognize the specific partner. The Fc fragment is the stem of the "Y", consisting of two heavy chains [33]. This structure is shown in Figure 5.1. This is the most abundant immunoglobulin and provides protection to the body by binding many kinds of pathogens, for example viruses, bacteria, and fungi with high affinity.

Antibody immobilization and IgG-Anti-IgG binding

As discussed in Chapter 4.1.2, after the surface modification by ESA thin films, biomolecules could be attached to the sensor head without denaturation and loss of biological activity. Immobilization methods can be classified as physical adsorption, covalent attachment, biomolecular interactions and host matrix encapsulation, among which physical adsorption is the simplest method for immobilizing biomolecules onto the sensor surface [34]. Antibodies can

be adsorbed onto the polymer thin films by hydrophobic and electrostatic interactions [35].

Hydrogen bonds, as well as hydrophobic interactions and electrostatic interactions, are the major interactions between antibody and antigen. The specificity of antibody and antigen binding is used as the sensing mechanism for the immunosensing.

In this report, the protein adsorption onto the MMF sensor surface upon the surface modification with self-assembled polyelectrolyte thin films is discussed. In addition, immunotest on commercially available IgG and anti-IgG is also investigated.

5.2 Immobilization of IgG on polymer thin film

5.2.1 Materials and methods

Materials and solution preparation

The materials used for this experiment as well as the solution preparation are described below. The salt concentration was adjusted by NaCl. A Corning 455 Ion Analyzer with ATC probe was used to adjust pH values with HCl and NaOH. HEPES buffered solution was applied for the pig IgG. The concentration of IgG solution was chosen based on previous research on effect of IgG concentration on immobilization [14]. 50 $\mu g/ml$ in concentration is high enough to get the expected thickness of an IgG monolayer. All experiments were carried out at room temperature. The substrate is the 50-micron silica as before.

The process of the immobilization experiment

1. "Piranha bath". The sensor was immersed in the piranha solution (Chapter 4.2.1) for 1 hour at room temperature, followed by ultrasonic rinsing and nitrogen drying.

2. ESA thin film fabrication for surface modification. PAH and PSS layers were adsorbed

Table 5.1: The materials used in the IgG immobilization experiment.

Material	**Detail**	**Company**
PAH	Polyallylamine hydrochloride	Aldrich
PSS	Polysodium 4-styrenesulfonate	Aldrich
HEPES	4-(2-hydroxyethyl)-1-piperazineethanesulfonic acid buffer, 1M	Fisher
IgG	Pig Immunoglobulin G, 1.0$\mu g/ml$	Bethyl Inc.

Table 5.2: The preparation of solutions for immobilization experiment.

Solution	**Volume**	**Concentration**	**Salt Concentration**	**pH**	**HEPES**
PAH	20 ml	4 mg/ml	0.15 M	7.5	
PSS	20 ml	4 mg/ml	0.15 M	7.5	
IgG	1 ml	50 $\mu g/ml$	0.15 M	7.36	0.05M

on the silica surface by alternately immersing the sensor in the polymer solutions, 5 min for each. Sensor was rinsed in ultrapure water for 2 min and dried in air for each layer. In order to study the mechanism of IgG adsorption onto the thin films, two test films were built up. A negatively charged $[PAH/PSS]_5$ film was formed for test 1 and a positively charged $[PAH/PSS]_5$PAH for test 2.

3. IgG immobilization. The sensor was immersed in pig IgG solution for 1 hour, followed by rinsing and drying. Then monolayer thickness was measured.

5.2.2 Results and analysis

The mechanism of IgG adsorption onto the polymer thin films is mainly by hydrophobic and electrostatic interactions. For test 1, there was a 10.4 nm optical thickness change when IgG was immobilized on the $[PAH/PSS]_5$ thin film. IgG adsorbed onto the $[PAH/PSS]_5$PAH layer yields a thickness change of 8.2 nm. This shows that the IgG could adsorb on both positively and negatively charged film layers.

The HEPES solution used for IgG adsorption was at pH 7.36. Since IgG has an isoelectric point around pH 6.8, IgG is negatively charge at pH 7.36 in this test, indicating the adsorption may not be driven by electrostatics since the outermost PSS layer is also negatively charged [31]. In respect that electrostatic force may not be the main factor influences the adsorption of IgG, it is possible that the adsorption is dominated by hydrophobic interaction. The exact mechanism of IgG adsorption is uncertain. However, ESA polymer thin film exhibits an effective precursor substrate for IgG immobilization.

We chose $[PAH/PSS]_5$ to be the precursor layer for IgG immobilization because higher thickness can be generated based on the result of the two tests. For $[PAH/PSS]_5$ film, the immobilization of IgG results in an overall optical thickness increment of 9.3 ± 0.5 nm (Figure 5.4).

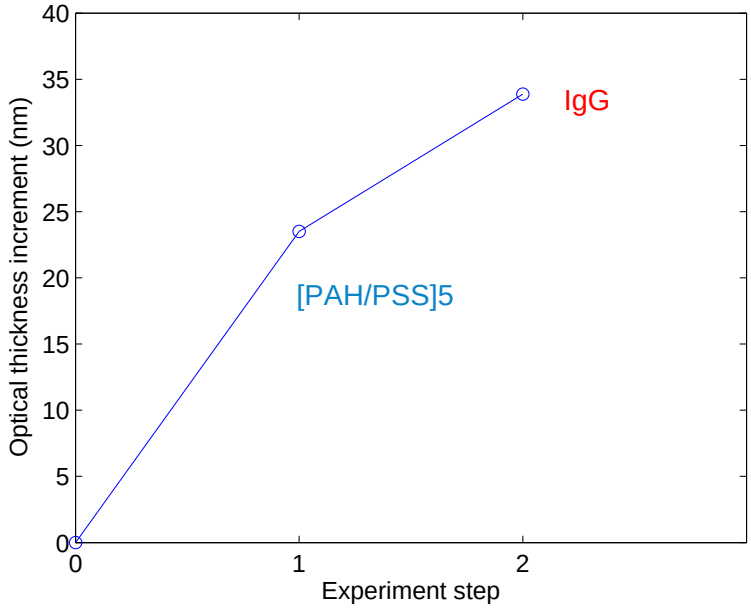

Figure 5.2: The adsorption of IgG on $[PAH/PSS]_5$.

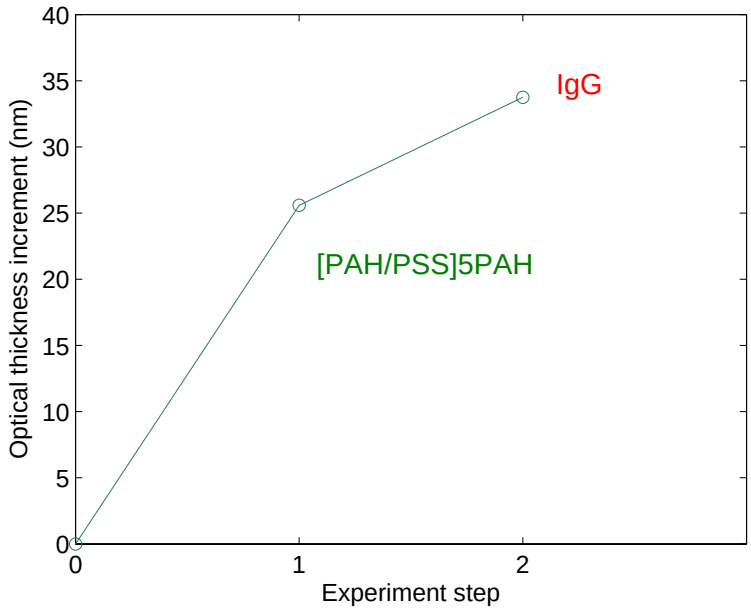

Figure 5.3: The adsorption of IgG on $[PAH/PSS]_5PAH$.

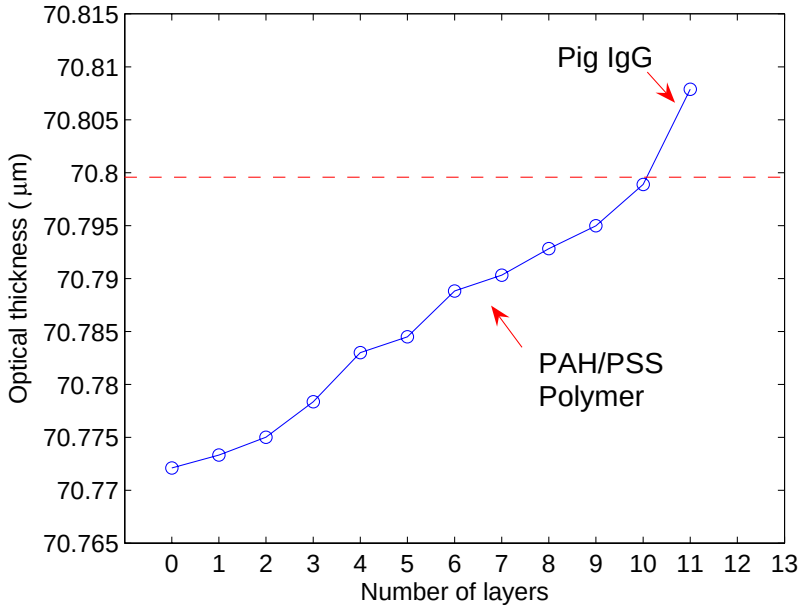

Figure 5.4: Change in optical thickness after the immobilization of IgG on ESA thin film ($[PAH/PSS]_5$).

5.3 Specific and nonspecific binding of anti-IgG

The immobilization of IgG enables the MMF-EFPI sensor to biosensing. The experiments were carried out to test the immunosesning ability of the sensor. Both specific binding and nonspecific binding were evaluated.

5.3.1 Materials preparation

The materials and solution preparation are shown in Table 5.3 and Table 5.4. The preparations were similar to those in immobilization experiment (Chapter 5.2.1). HEPES buffered solution was applied for all the IgG and anti-IgGs. A standard binding block solution (2% bovine serum albumin(BSA)) was applied in the last experiment to reduce the nonspecific binding citer5.05.

Table 5.3: The materials used in the immunosensing experiment.

Material	**Detail**	**Company**
PAH	Polyallylamine hydrochloride	Aldrich
PSS	Polysodium 4-styrenesulfonate	Aldrich
HEPES	4-(2-hydroxyethyl)-1-piperazineethanesulfonic acid buffer, 1M	Fisher
Pig IgG	Immunoglobulin G, $1.0 \mu g/ml$	Bethyl Inc.
Anti-pig IgG	$1.0 \mu g/ml$	Bethyl Inc.
Anti-rabbit IgG	$1.0 \mu g/ml$	Bethyl Inc.
BSA	Bovine serum albumin, crystal	

Table 5.4: The preparation of solutions for immunosensing experiment.

Solution	**Volume**	**Concentration**	**Salt Concentration**	**HEPES**
PAH	20 ml	4 mg/ml	0.15 M	
PSS	20 ml	4 mg/ml	0.15 M	
Pig IgG	1 ml	50 $\mu g/ml$	0.15 M	0.05M
Anti-pig IgG	1 ml	25 $\mu g/ml$	0.15 M	0.05M
Anti-rabbit IgG	1 ml	25 $\mu g/ml$	0.15 M	0.05M
Standard binding block	2 ml	2% BSA		

5.3.2 Experimental process and result

Anti-pig IgG binding to pig IgG

1. ESA thin films. $[PAH/PSS]_5$ was first deposited onto the sensor to form a precursor film for IgG binding.

2. IgG immobilization. Sensor was immersed in pig IgG solution for 1 hour, followed by rinsing and drying. The immunosensor was fabricated after this process.

3. Anti-pig IgG binding. The immunosensor was exposed to anti-pig IgG prepared in HEPES buffer for 1 hour. Data was collected after the rinsing and drying process.

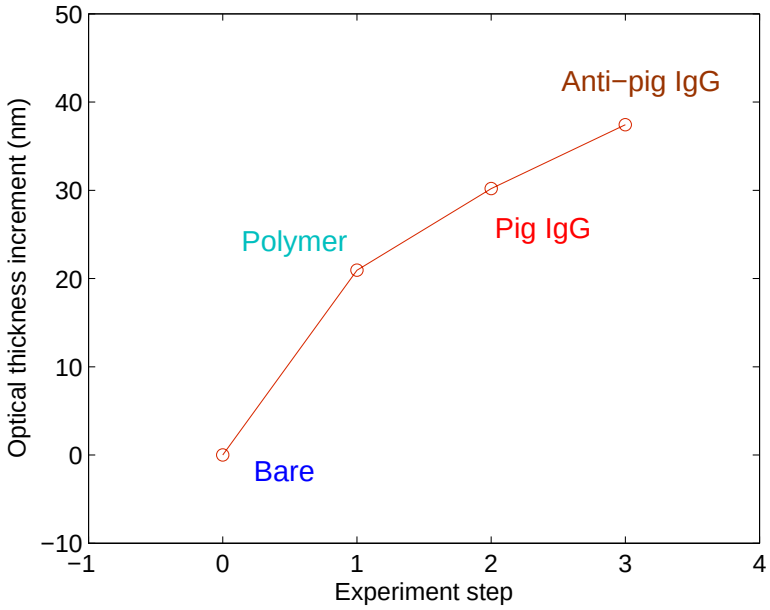

Figure 5.5: Change in optical thickness after the immobilization of IgG on ESA thin films, and the binding of anti-pig IgG.

All the experiment steps were monitored by the MMF sensor and the white-light system. Film thickness was measured after the adsorption of each layer. The binding of anti-pig IgG resulted in an optical thickness increment of 8.8 nm (Figure 5.5). Hydrogen bonds, hydrophobic interactions, and electrostatic interactions contribute to the binding.

Anti-rabbit IgG binding to pig IgG

1. ESA thin films. $[PAH/PSS]_5$ was first deposited onto the sensor as in the specific binding test.

2. Pig IgG immobilization. Sensor was immersed in pig IgG solution for 1 hour, followed by ultrasonic rinsing and drying.

3. Anti-rabbit IgG binding. The immunosensor was immersed in anti-rabbit IgG solution, other than anti-pig IgG, for 1 hour. Data was collected after the rinsing and drying process.

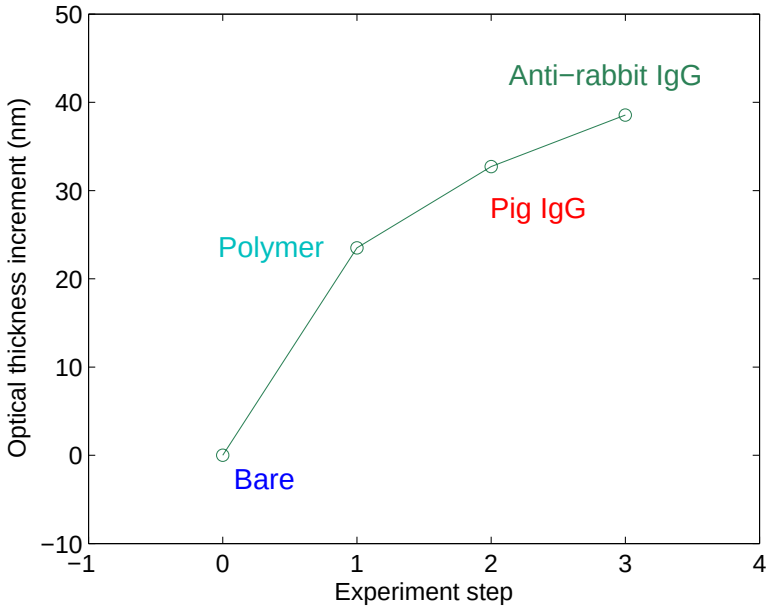

Figure 5.6: Change in optical thickness after the immobilization of IgG on ESA thin films, and the binding of anti-rabbit IgG.

The nonspecific binding of anti-rabbit IgG generated an increment of 7.9 nm in optical thickness, which shows that the cross interaction took place when nonspecific anti-IgG was applied. Analytes bind to other sites in addition to binding to receptors of interest. The nonspecific binding may due to the adsorption of anti-IgG to the uncovered precursor film

other than the Fab fragments of IgG. As the key issue in immunosensing, specificity of the biosensor is important in the immnuno tests. Therefore, a binding block process as the pre-treatment is needed to reduce the nonspecific binding.

Anti-IgG binding to IgG when binding block is applied

1. ESA thin films. $[PAH/PSS]_5$ thin film was first fabricated on the sensor head.
2. Pig IgG immobilization. Sensor was immersed in pig IgG solution for 1 hour to fabricate an IgG monolayer.
3. Binding block process. BSA was applied to reduce the nonspecific binding. Sensor was immersed into BSA solution for 1 hour and relative optical thickness was obtained.
4. Anti-rabbit IgG binding. The sensor was immersed in anti-rabbit IgG solution for 1 hour for non-specific binding. Data was recorded.
5. Anti-pig IgG binding. Dip the sensor in anti-pig IgG solution for another 1 hour to examine the specific binding.

After the IgG immobilization, an optical thickness increment of 4.5 nm occurred for the BSA layer. The binding of anti-rabbit IgG to immobilized pig IgG resulted in only 1.3 nm in thickness change compared with that of 8.0 nm after anti-pig IgG binding. According to this difference, nonspecific binding represents a much lower level than the specific binding when binding block is applied.

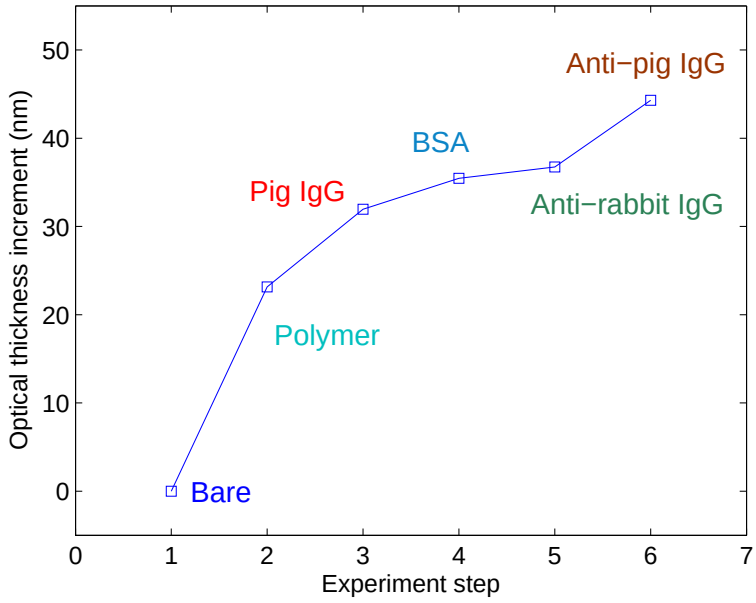

Figure 5.7: Change in optical thickness after the immobilization of IgG on ESA thin films, binding block process (BSA: boviene serum albumin), the binding of anti-rabbit IgG and anti-pig IgG.

5.4 Conclusion

IgG immobilized onto the sensor head displays an effective binding with polymer ESA thin films previously applied as a protective substrate. The biological sensing function was retained. The adsorption of IgG onto both positively and negatively charged polymer films was examined. $[PAH/PSS]_5$ was chosen to be the precursor layer for IgG immobilization due to higher thickness generated.

The results of immunosensing experiment verified that the MMF-EFPI sensor could be used as a biosensor. Both specific binding and nonspecific binding were investigated. Binding block was applied prior to testing, in which case specific binding exhibited a much higher level than nonspecific binding.

Chapter 6

Conclusions and future work

Conclusions

To fulfill the objective of making multimode fiber optic sensors capable of biosensing, this thesis presents a detailed research work on the development, fabrication and measurement of multimode fiber (MMF) extrinsic Fabry-Perot interferometric (EFPI) biosensor.

Based on EFPI technology, a MMF sensor has been developed and fabricated. The sensor was interrogated by the Ocean-Optics spectrometer-based white-light system. The experimental setup of the whole system is easy and inexpensive and high signal visibility can be obtained. The application of this MMF-EFPI sensor in biosensing has been evaluated.

ESA technology was successfully applied on the MMF sensor. The progress of polymer self-assembled thin film growth was investigated by the sensor and the white-light system. ESA thin films are an effective tool in surface modification to protect the biological activity of bioreceptors on the optical fiber biosensor.

IgG deposited on a PAH/PSS polymer layer exhibits effective immobilization, allowing the sensor to be used for immunosensing. Both specific binding and nonspecific binding have been investigated. Each step of the immobilization experiment and binding experiment was

evaluated. Layer thickness could be measured by the system. Binding between IgG and corresponding anti-IgG, and cross interaction between the non related pair were evaluated, showing the higher level of specific binding.

Future work

It is evident that the MMF-EFPI sensor could find its application in other aims such as bacterial detection and DNA detection. In bacterial detection, cell dimensions are usually of micrometers and cells are sparsely immobilized, which make it difficult to detect the bacterial by a single mode fiber (SMF) sensor since the detection area (the core) is rather small. As for a MMF sensor, the sensing area is largely increased due to the larger core size of the MMF sensor. The fiber used in this research is a 50/125 μm multimode optical fiber, which could be switched to a 105/125 μm multimode fiber to further enlarge the sensing area.

Bibliography

[1] D. A. Krohn, *Fiber optic sensors fundamentals and applications*, 3rd ed, Instrument society of America, 2000.

[2] Mohammad Llyas, Hussein T. Moustah, *The Handbook of Optical Communication Networks*, CRC Press: Boca Raton, London, New York, Washinton, D.C., 2003.

[3] Xiaopei Chen, *Fiber Optic Pressure Sensor Fabrication Using MEMS Technology*, M. S. thesis, The Bradley Department of Electrical Engineering, Virginia Tech, Blacksburg, Virginia, April, 2003.

[4] D. A. Jackson, "Recent progress in monomode fibre-optic sensors," *Meas. Sci. Technol.* **5,** 621-638, 1994.

[5] Francis T.S. Yu, Shizhuo Yin, *Fiber Optic Sensors*, Marcel Dekker, Inc. New York, 2002.

[6] J. E. Chong, L. Leija, C. P. Pennisi, and W. H. Fonseca, "Optical Fiber Based Thermometry System for A Hyperthermia Laboratory," *Proceedings of the 23rd Annual EMBS International Conference*, October 25-28, 2001.

[7] Kentaro Hase, Shuhei Sakai, Kosuke Tsukada, Eiichi Sekizuka, Chikara Oshio, Haruyuki Minamitani, "Continuous Measurement of Blood Oxygen Pressure Using a Fiber Optic Sensor Based on Phosphorescence Quenching," *Proceedings of the 2nd Joint EMBS/BMES Conference*, Houston, TX, USA, Oct. 23-26, 2002.

[8] Jiusheng Li, Zhenwu Bao, "Application of the Neural Network Optical Fiber Temperature Sensor Probe Design Used in Medical Treatment," *IEEE Int. Conf. Neural Networks and Signal Processing*, Nanjing, China, December 14-17, 2003.

[9] Q. Chen, R. O. Claus, W. B. Spillman, F. J.Arregui, I. R. Matias, and K. L. Cooper, "Optical Fiber Sensors for Breathing Diagnostics," *Optical Fiber Sensors Conference Technical Digest*, 2002.

[10] Yoshiaki Sasaki, Shinji Tanosaki, Jota Suzuki, Tetsuya Yuasa, Hiroshi Taniguchi, Balasigamani Devaraj, and Takao Akatsuka, "Fundamental Imaging Properties of Transillumination Laser CT Using Optical Fiber Applicable to Bio-Medical Sensing," *IEEE Sensors Journal*, Vol. 3, NO. 5, October 2003.

[11] Clark, L.C., Jr. and Lions, C., "Electrode systems for continuous monitoring in cardiovascular surgery," Ann. N.Y. *Acad. Sci.*, 102, 29, 1962.

[12] Braguglia, C.M., "Biosensors: an outline of general principles and application," *Chem. Biochem. Eng.*, Q., 12, 183, 1998.

[13] Tuan Vo-Dinh, "Chapter 20, Biosensors for Medical Application," *Biomedical Photonics Handbook*, CRC Press, 2002.

[14] Yan Zhang, *Miniature fiber-optic multicavity Fabry-Perot interferometric biosensor*, Ph.D. dissertation, The Bradley Department of Electrical Engineering, Virginia Tech, Blacksburg, Virginia, December 6, 2005.

[15] C.E.Lee, Henry F. Taylor, *Optical Fiber Fabry-Perot Sensors.*

[16] Henry F. Taylor, "Fiber Optic Sensors Based upon the Fabry-Perot Interferomete," *Fiber Optic Sensors*, Marcel Dekker, Inc. New York, 2002.

[17] Yizheng Zhu, Zhengyu Huang, Fabin Shen, and Anbo Wang, "Sapphire-fiber-based white-light interferometric sensor for high-temperature measurements," *Optics Letters*, Vol. 30, No. 7, April, 2005.

[18] R. E. Wagner, and C. R. Sandahl, "Interference effects in optical fiber connections," *Appl. Opt.* 21, 1381-1385, 1982.

[19] F. Perennes, P. C. Beard, and T. N. Mills, "Analysis of a low-finesse Fabry-Perot sensing interferometer illuminated by a multimode optical fiber", *Appl. Opt.* 38, 7026-7024, 1999.

[20] Ming Han, *Theoretical and Experimental Study of Low-Finesse Extrinsic Fabry-Perot Interferometric Fiber Optic Sensors*, Ph.D. dissertation, The Bradley Department of Electrical Engineering, Virginia Tech, Blacksburg, Virginia, May, 2006.

[21] Bing Qi, Gary R. Pickrell, JunCheng Xu, Po Zhang, Yuhong Duan, Wei Peng, Zhenyu Huang, Wei Huo, Hai Xiao Russell G. May, Anbo Wang, "Novel data processing techniques for dispersive white light interferometer," *Opt. Eng.* 42(11), 3165-3171, November, 2003.

[22] Yunfeng Lu, *Self-assembled nanostructured materials : symposium held April 22-25, 2003, San Francisco, California, U.S.A.*.

[23] A. Ulman, *An Introduction to Ultrathin Organic Films, From Langmuir-Blodgett to Self-Assembly*, Academic Press: New York, 1991.

[24] Kristie Lenahan Cooper, *Electrostatic Self-Assembly of Linear and Nonlinear Optical Thin Films*, Ph.D. dissertation, The Bradley Department of Electrical Engineering, Virginia Tech, Blacksburg, Virginia, April, 1999.

[25] G. Decher, J.D. Hong, and J. Schmitt, "Buildup of Ultrathin Multilayer Films by a Self-Assembly Process .3. Consecutively Alternating Adsorption of Anionic and Cationic Polyelectrolytes on Charged Surfaces," *Thin Solid Films*, 1992. 210(1-2): p. 831-835.

[26] G. Decher, Y. Lvov and J. Schmitt, "Proof of multilayer structural organization in slefassembled polycation-polyanion molecular films," *Thin Solid Films*, 244, 772 1994.

[27] G. Decher, and J. Schmitt, "Fine-tuning of the film thickness of ultrathin multilayer films composed of consecutively alternating layers of anionic and cationic polyelectrolytes," *Prog. Colloid Polym. Sci.*, 1992. 89 p. 160-164.

[28] G. Decher, and J.B. Schlenoff, *Multilayer thin films: sequential assembly of nanocomposite materials*, 2003, Weinheim Cambridge: Wiley-VCH.

[29] Brillhart, K. L.; Ngo, T. T. *J. Immunol. Methods*, 1991, 144, 19.

[30] Iler, R.K., *The chemistry of silica: solubility, polymerization, colloid and surface properties, and biochemistry*, 1979, New York: Wiley.

[31] Caruso, F., et al., "2. Assembly of alternating polyelectrolyte and protein multilayer films for immunosensing," *Langmuir*, 1997. 13(13): p. 3427-3433.

[32] http://en.wikipedia.org/wiki/IgG

[33] Harlow, E. and D. Lane, *Using antibodies: a laboratory manual*, Cold Spring Harbor Laboratory Press, New York, 1999.

[34] Giacomelli, C.E., "Adsorption of immunoglobulins at solid-liquid interfaces," in *Encyclopedia of Surface and Colloid Science*, A.T. Hubbard, Editor. 2002, Marcel Dekker: New York. p. 418-439.

[35] Buijs, J., et al., "Adsorption dynamics of IgG and its F(ab')(2) and Fc fragments studied by reflectometry," *J. Colloid Interface Sci.*, 1996. 178(2): p. 594-605.

[36] Yan Zhang, Helen Shibru, Kristie L. Cooper, Anbo Wang, "A miniature fiber optic Multi-cavity Fabry-Perot interferometric biosensor," *Opt. Lett.*, 2005. 30(9): p. 1021-1023.

Vita

Xin Zhao was born on March 22, 1981 in Hubei, China. She graduated from Huazhong University of Science and Technology with a Bachelor of Science in Biomedical Engineering in June 2003. Ms. Zhao continued her M.S. study in the Bradley Department of Electrical Engineering of Virginia Polytechnic Institute and State University (Virginia Tech) from August 2004. She was a Graduate Research Assistant in the Center for Photonics Technology (CPT) at Virginia Tech, where her research was focused on fiber optic biosensor and molecular self-assembly.